A&A 466, 667–673 (2007)
DOI: 10.1051/0004-6361:20066647

Astronomy & Astrophysics

Vertical abundance stratification in the blue horizontal branch star HD 135485⋆,⋆⋆

V. R. Khalack[1,2], F. LeBlanc[1], D. Bohlender[3], G. A. Wade[2], and B. B. Behr[4,⋆⋆⋆]

[1] Département de Physique et d'Astronomie, Université de Moncton, Moncton, N.-B., E1A 3E9, Canada
e-mail: khalakv@umoncton.ca
[2] Department of Physics, Royal Military College of Canada, PO Box 17000 stn 'FORCES', Kingston, Ontario, K7K 4B4, Canada
[3] National Research Council of Canada, Herzberg Institute of Astrophysics, 5071 West Saanich Road, Victoria, BC, V9E 2E7, Canada
[4] Department of Astronomy, University of Texas at Austin, 1 University Station C1400, Austin TX 78712-0259, USA

Received 26 October 2006 / Accepted 29 January 2007

ABSTRACT

Context. It is commonly believed that the observed overabundances of many chemical species relative to the expected cluster metallicity in blue horizontal branch (BHB) stars appear as a result of atomic diffusion in the photosphere. The slow rotation of BHB stars (with $T_{\rm eff} > 11\,500$ K), typically $v \sin i < 10$ km s^{-1}, is consistent with this idea.
Aims. In this work we search for observational evidence of vertical chemical stratification in the atmosphere of HD 135485. If this evidence exists, it will demonstrate the importance of atomic diffusion processes in the atmospheres of BHB stars.
Methods. We undertake an extensive abundance stratification analysis of the atmosphere of HD 135485, based on recently acquired high resolution and S/N CFHT ESPaDOnS spectra and a McDonald-CE spectrum.
Results. Our numerical simulations show that nitrogen and sulfur reveal signatures of vertical abundance stratification in the stellar atmosphere. It appears that the abundances of these elements increase toward the upper atmosphere. This fact cannot be explained by the influence of microturbulent velocity, because oxygen, carbon, neon, argon, titanium and chromium do not show similar behavior and their abundances remain constant throughout the atmosphere. It seems that the iron abundance may increase marginally toward the lower atmosphere. This is the first demonstration of vertical abundance stratification of metals in a BHB star.

Key words. stars: atmospheres – stars: horizontal-branch – stars: chemically peculiar – stars: individual: HD 135485

1. Introduction

HD 135485 appears to be an evolved star that lies close to or on the horizontal branch (Trundle et al. 2001). It has mid-B spectral type and shows many prominent absorption lines of metallic species in its spectrum. The most recent absolute and differential abundance analysis of HD 135485 was performed by Trundle et al. (2001). They found a large (0.5−1.0 dex) enhancement of metal abundances in comparison with the solar composition. Similar results were obtained previously by Schönberner (1973) and Dufton (1973) from analysis of moderate-resolution photographic spectra. In an attempt to explain the anomalous chemical composition in the atmosphere of HD 135485, Dufton (1973) considered the possibility of binary system evolution, where the mass flow onto HD 135485 from a high mass component may have created the observed enhancements of metal species. In order to try to prove this hypothesis, Dufton investigated the radial velocity during a five month period, but found no variation (see Trundle et al. 2001, for details).

Another possible explanation proposed for the unusually high metallicity is that the star was formed in a region of high metallicity, such as the Galactic Center, and during the long period of its stellar evolution it could have traveled over a large distance (∼26 kpc) as demonstrated by Trundle et al. (2001) from analysis of the kinematical properties of HD 135485.

Together with general enrichment of all metals (except nickel which is significantly depleted) with respect to hydrogen, Trundle et al. (2001) have also found a slightly enhanced helium abundance of ∼0.3 dex. They interpret this fact along with the anomalously high (∼1.3 dex) nitrogen overabundance as an indication that the carbon-nitrogen (CN) cycle took place during the hydrogen-burning phase on the main sequence. The relatively normal carbon enhancement might reflect a balance between its being destroyed by the CN cycle and created via helium core flashes during the red giant phase (which could also explain the observed neon enrichment in the atmosphere). These facts and the present position of HD 135485 on the Hertzsprung-Russell (HR) diagram argue that this star is evolved and probably belongs to the blue horizontal branch (BHB) stars. The observed low (projected) rotational velocity ($v \sin i < 4$ km s^{-1}) of HD 135485, the observed chemical peculiarities (except the helium enrichment) and the effective temperature $T_{\rm eff} = 15\,500$ K (Trundle et al. 2001) are typical for BHB stars.

Comprehensive surveys of BHB star abundances show that the stars hotter than $T_{\rm eff} \simeq 11\,500$ K have abundance anomalies

⋆ Based on observations made with ESPaDOnS at the Canada-France-Hawaii Telescope (CFHT) operated by the National Research Council (NRC) of Canada, the Institut des Sciences de l'Univers of the Centre National de la Recherche Scientifique (CNRS) and the University of Hawaii and on observations made with Echelle Spectrograph on the McDonald Observatory 2.1-m Otto Struve Telescope.
⋆⋆ Full Table 2 is only available in electronic form at http://www.aanda.org
⋆⋆⋆ *Current address*: US Naval Observatory, 3450 Massachusetts Avenue NW, Washington DC 20392, USA.

Table 1. Journal of spectroscopic observations of HD 135485.

Date (UT)	HJD (2 450 000 +)	Instrument	t_{exp} (s)	S/N ratio (pixel)$^{-1}$	Coverage λ (Å)	Resolution
2001 Mar. 09	1978.9242	CE	600	67	4760–5570	60 000
2005 May 19	3509.8677	ESPaDOnS	600	150	3720–10 290	80 000
2005 May 19	3509.8753	ESPaDOnS	600	140	3720–10 290	80 000

when compared to the BHB stars of lower effective temperature in the same cluster[1] (Glaspey et al. 1989, Grundhal et al. 1999). Also, Peterson et al. (1995); Behr et al. (2000) and Recio-Blanco et al. (2004) showed the existence of a discontinuity in stellar rotation velocity distribution of BHB stars at $T_{\rm eff} \simeq 11\,500$ K. All of the hotter stars show modest rotation ($v \sin i < 10\,{\rm km\,s^{-1}}$), while the cooler stars are rotating more rapidly.

Other observational results show both photometric jumps (Grundhal et al. 1999) and photometric gaps (Ferraro et al. 1998), also occurring at $T_{\rm eff} \simeq 11\,500$ K, as well as low measured surface gravities. The low gravity, abundance anomalies and slow rotation suggest that microscopic atomic diffusion is effective in stellar atmospheres of the BHB stars with $T_{\rm eff} \geq 11\,500$ K. In this picture, the competition between radiative acceleration and gravitational settling yields a net acceleration on atoms, which results in their diffusion through the atmosphere. A consequence of this process is vertically-stratified abundances of chemical elements. The aim of this paper is to attempt to detect observationally such vertical stratification of elements in the atmospheres of BHB stars. Direct measurement of this stratification from line profile analysis would provide a convincing argument in favour of efficient chemical diffusion in the atmospheres of BHB stars with $T_{\rm eff} \geq 11\,500$ K.

The most important difference between HD 135485 and most BHB stars is that it has an enhanced helium abundance. Therefore HD 135485 might be a very young BHB star in which helium has not yet settled. However, a detailed investigation of this possibility is outside the scope of this paper.

To verify if the abundances of some chemical species are vertically stratified in the atmosphere of HD 135485, we undertook a detailed analysis of available high-resolution spectra employing a modification of the approach for abundance stratification analysis developed by Ryabchikova et al. (2005). In Sect. 2 we discuss the properties of the observed spectra, and in Sect. 3 we describe the atmospheric parameters of HD 135485 and modelling details. The results of abundance determinations are considered in Sect. 4, while a description of vertical stratification for some chemical species is shown in Sect. 5. A discussion of our results follows in Sect. 6.

2. Observations

Spectroscopic observations of HD 135485 were undertaken in March 2001 and May 2005. The journal of spectroscopic observations is shown in Table 1, where individual columns give the UT date of the observation, heliocentric Julian Date of the observation, the instrument specification, exposure time, signal-to-noise (S/N) ratios per pixel (the peak typically occurs around 5400 Å), spectral coverage and resolving power (which depends on central wavelength).

[1] Most of the known BHB stars are found in globular clusters.

2.1. McDonald Cassegrain Echelle spectrum

The first spectrum of HD 135485 (from Table 1) was obtained in the framework of a study of the rotational characteristics ($v \sin i$) of BHB stars (Behr 2003) using the Cassegrain Echelle (CE) Spectrograph (McCarthy et al. 1993) on the McDonald Observatory 2.1-m Otto Struve Telescope. This instrument provides a nominal resolving power of $R \sim 60\,000$. The signal-to-noise ratio (per pixel) was computed from the reduced spectrum by smoothing the spectral regions identified as continuum, and then computing the rms deviation between the observed and smoothed spectra.

The package of routines developed by McCarthy (1990) for the FIGARO data analysis package (Shortridge 1993) was employed to reduce the spectrum. The detailed description of the reduction procedure for this particular spectrum, including the wavelength calibration routine and the continuum normalization, is provided by Behr (2003). The procedure follows a standard prescription, with bias subtraction, flat-fielding, order extraction, and wavelength calibration from thorium-argon arc lamp observations. Cosmic ray hits were identified and removed by hand for maximum spectral quality. No smoothing was applied to the spectra.

2.2. CFHT-ESPaDOnS spectra

The other two spectra were obtained using the new ESPaDOnS (Echelle SpectroPolarimetric Device for Observations of Stars) spectropolarimeter at the Canada-France-Hawaii Telescope (CFHT). ESPaDOnS is fundamentally similar in construction to the MuSiCoS spectropolarimeter (Donati et al. 1999) and allows the acquisition of an essentially continuous spectrum throughout the spectral range 3700 Å to 10 500 Å in a single exposure. The optical characteristics of the spectrograph as well as the spectropolarimeter observing procedures, are described by Donati et al. (in preparation)[2]. Observations were performed in the spectroscopic "sky only" mode of the instrument that provides the highest resolving power ($R \sim 80\,000$). This resolution corresponds to velocity elements of 3.75 km s^{-1}.

The ESPaDOnS spectra were reduced using the Libre-ESpRIT reduction tool (Donati et al., in preparation), which is the most recent release of ESpRIT (Donati et al. 1997). The continuum of each spectral order was normalized by fitting a 3rd to 5th order polynomial (as selected by eye) to regions free of prominent spectral lines and not located immediately at the beginning or at the end of the spectral order.

3. Line profile simulations

3.1. Stellar atmosphere parameters

The line profile simulations were performed using a Phoenix (Hauschildt et al. 1997) LTE (Local Thermodynamic

[2] For more details about this instrument, the reader is invited to visit www.ast.obs-mip.fr/projects/espadons/espadons.html

Equilibrium) stellar atmosphere model with enhanced (+1.0 dex) metallicity. The model is calculated assuming $T_{\rm eff}$ = 15 500 K, and $\log g$ = 4.0, which according to Trundle et al. (2001) provide the best description of observable line profiles of HD 135485. Those authors adopted a microturbulent velocity of 5 km s^{-1} to provide a constant behavior of abundances over the range of equivalent widths measured for sulfur and nitrogen ions. Behr (2003) has adopted for this star ξ = 1.4 km s^{-1} and obtained $v \sin i$ = 0 km s^{-1}.

From our perspective, the physical motivation for adopting a microturbulent velocity is unclear. According to Landstreet (1998), photospheric convection should be very weak at the effective temperatures of BHB stars. Landstreet found that spectroscopically-derived microtubulence had decreased from around 4 km s^{-1} in late A stars with $T_{\rm eff} \sim$ 8000 K to 0.5 km s^{-1} in early A stars with $T_{\rm eff} \sim$ 10 500 K. In particular, strong microtubulence (e.g. 5 km s^{-1} as adopted by Trundle et al. 2001) should be accompanied by strong line asymmetries, which we do not observe. We therefore realistically expect no detectable microturbulence in HD 135485. Of course, Landstreet's analysis was performed for main sequence stars; we might reasonably expect that BHB stars show some differences, although the atmospheric parameters of HD 135485 are very similar to those of main sequence stars.

Based on this guidance, we have tentatively adopted a microturbulent velocity 0 km s^{-1} for our abundance analysis of HD 135485. Using zero microturbulence in spectral synthesis we estimated stellar rotational velocity $v \sin i$ = 2−3 km s^{-1}. This is an important assumption for several reasons. First, because diffusion is a slow process, the mixing which might be implied by the presence of microturbulence could serve to reduce or erase chemical stratification. Also, adoption of microturbulence modifies line strengths, leading to systematic changes in inferred mean abundances as well as abundance trends with line strength. As we shall see in Sect. 5, the validity of the assumption of zero microturbulence can be tested, and it is fully consistent with our spectroscopic observations.

3.2. Procedure

All of the available spectra were examined to compose a line list for chemical species that are suitable for abundance and stratification analysis. The line identification is performed using the VALD-2 (Kupka et al. 1999; Ryabchikova et al. 1999) and NIST[3] (version 3.0.3) line databases (Reader et al. 2002). The same sources are used to specify the atomic data for the selected lines. For Fe II and Cr II lines we extracted atomic data from Raassen & Uylings[4] (1998), while for some Fe II lines we also used the atomic data recently obtained by Fuhr & Wiese (2006). An example of the first ten lines from the line list selected for the abundance analysis of N II lines is shown in Table 2[5], where references identify sources for the adopted $\log gf$ values, while the given energy levels are taken mostly from the NIST database.

All line profiles are simulated using the ZEEMAN2 spectrum synthesis code (Landstreet 1988; Wade et al. 2001) assuming Gaussian instrumental profiles. The stability of the ESPaDOnS instrumental profile has been investigated using the calibration spectra of a ThAr quartz lamp. We find the instrumental profile to be stable during the night of observation and to reveal no

[3] http://physics.nist.gov/PhysRefData/ASD/index.html

[4] ftp://ftp.wins.uva.nl/pub/orth

[5] Full Table 2 is presented in the electronic edition of the journal. A portion is shown here for guidance and content.

Table 2. List of spectral lines used for the abundance analysis.

N II				
λ, Å	$\log gf$	E_i, cm^{-1}	$\log \gamma_{\rm rad}$	Ref.
4447.030	0.228	164 610.76	9.16	NIST
4507.556	−0.817	166 678.64	9.33	VALD
4601.478	−0.428	148 940.17	9.23	VALD
4613.868	−0.665	148 940.17	9.23	VALD
4621.396	−0.514	148 940.17	9.23	VALD
4630.539	0.094	149 076.52	9.15	VALD
4779.722	−0.587	166 521.69	9.58	VALD
4803.287	−0.113	166 678.64	9.58	VALD
4987.376	−0.555	168 892.21	9.34	VALD
4994.367	−0.069	168 892.21	9.34	VALD

dependence on the intensity of the line profile. The ZEEMAN2 code has been modified (Khalack & Wade 2006) to allow for an automatic minimization of the model parameters using the *downhill simplex method* (Press et al. 1992). The relatively poor efficiency of the downhill simplex method, requiring a large number of function evaluations, is a well known problem. Repeating the minimization routine several times in the vicinity of a supposed minimum in the parameter space allows us to check if the method converges to the global minimum.

To search for the presence of abundance stratification, we have used two different methods. In the first method, we estimate the abundance of a chemical element from independent analysis of each line profile. For every layer of the stellar atmosphere model (it contains 50 layers) we calculate the line optical depth τ_ℓ in the line core. We suppose that each analyzed profile is formed mainly at τ_ℓ = 1, which corresponds to a particular layer of the stellar atmosphere. Finally, for this layer, the respective continuum optical depth τ_{5000} is specified. In this way, we have built the scale of optical depths τ_{5000} to track vertical abundance stratification through the analysis of all the available line profiles for a chosen chemical element.

Three free model parameters (the element's abundance, line radial velocity $V_{\rm r}$ and $v \sin i$) were derived from each line profile using the aforementioned automatic minimization routine. HD 135485 has very sharp absorption lines and even for resolution R = 80 000 a line profile usually consists of only 8 to 15 bins. This leads to the fact that the downhill simplex method fails to converge to the global minimum in approximately 2 to 5% of analyzed line profiles. This means that the automatic minimization routine remains in the vicinity of a local minimum and results in a higher final value of the χ^2-function. Repeating the minimization routine with different starting values of the model parameters usually solves this problem and provides a better fit, which is checked using a few additional runs of the simulation routine. Sometimes, analysis of a line profile results in a radial velocity which differs significantly from the average $V_{\rm r}$ = 4.2 km s^{-1} (obtained from analysis of all line profiles of the same chemical element and other chemical species). This may be evidence for line misidentifications or inaccurate line wavelengths. Therefore lines with radial velocities which differ more than 1.5 km s^{-1} from the average are not taken into account in the modeling and are not included in Table 2.

In the second method, we only analyzed those lines which appear to be good candidates in the previous approach and consider the two-step stratified abundance model with a linear transition zone (Ryabchikova et al. 2003; Wade et al. 2003) to describe the abundance distribution. In this case, all the selected lines were analyzed simultaneously and in the minimization

routine we operated with 6 free model parameters: the element's abundance in the deeper layers, the (standard) optical depth τ_1 of the transition zone lower (deeper) boundary (where the element's abundance begins its linear increase or decrease), the optical depth τ_2 of the transition zone upper boundary, the difference between the abundances at two boundaries, the stellar radial velocity and the $v \sin i$. We note that for the second method the downhill simplex method never failed to reach the global minimum. This means that information stored in all of the analyzed lines, modeled simultaneously, is statistically sufficient to provide a unique solution. To determine the averaged abundances for all of the analyzed chemical species, we simultaneously fit the available line profiles using the same three free model parameters used in the first approach.

Initially, we specify arbitrarily the free model parameters in the range of their possible values and simulate the line profiles. We then compare the simulated profiles with the observed spectra, and calculate the reduced χ^2, which we adopt as a measure of the fit quality. The expression for the χ^2 function, which reflects the agreement between the simulated profiles (I_{i,λ_j}) and observed spectra ($I^{\rm obs}_{i,\lambda_j}$) is given by:

$$\chi^2_I = \frac{1}{N_I} \sum_{i=1}^{N_I} \frac{1}{N_i} \sum_{j=1}^{N_i} \left(\frac{I^{\rm obs}_{i,\lambda_j} - I_{i,\lambda_j}}{\sigma[I^{\rm obs}_{i,\lambda_j}]} \right)^2, \quad (1)$$

where $\sigma[I^{\rm obs}_{i,\lambda_j}]$ corresponds to the measurement errors, N_I represents the number of profiles indexed by i, while N_i is the number of pixels in each analyzed line profile. In the first method of the analysis we used $N_I = 1$. In fact, the simulated spectra are calculated with a resolution of 0.01 Å and so do not provide a direct coincidence of wavelengths in the simulated and observed spectra. Therefore, during the χ^2 function evaluation the simulated spectral intensity at the exact observed wavelength is calculated using a linear interpolation.

In order to evaluate the fit errors (and therefore the uncertainties on the derived free parameters), we calculate deviations of the simulated profiles produced as a result of small variations of each of the free parameters, thus introducing a small shift along one axis in the χ^2 hyper-space from the point of the function minimum value. Using this procedure, and taking into account the uncertainties of the observational data and the obtained minimum value of the χ^2-function, we can estimate the errors of the best-fit parameters.

4. Results of abundance analysis

We have identified in the spectra of HD 135485 most of the lines reported by Trundle et al. (2001). No lines of Mn II and Ni II were detectable in our spectra and these elements were therefore not analysed. It seems that Trundle et al. (2001) have determined the Mn II and Ni II abundances from the much stronger ultraviolet lines of these species. The McDonald-CE spectrum has lower spectral resolution than the ESPaDOnS data and is used mainly to confirm the average abundance obtained with the ESPaDOnS spectra.

A preliminary LTE abundance analysis of helium lines suggests an enhanced helium abundance in HD 135485, and the element also seems to be vertically stratified. The helium overabundance obtained is in good agreement with the results reported by Trundle et al. (2001).

The mean photospheric abundances we derive for HD 135485 are reported in Table 3. The second and third columns contain respectively the mean abundance of the chemical species and the number of analyzed line profiles in the ESPaDOnS spectra, while the fourth and fifth columns represent similar results obtained from analysis of the McDonald-CE spectrum. The last column contains the solar atmospheric abundances recalculated from $\log(N/N_{\rm H})$ data (Asplund et al. 2005).

Table 3. Mean atmospheric abundances $\log(N/N_{\rm tot})$ of HD 135485 with uncertainties equal to the standard deviation of n measured lines.

	CFHT-ESPaDOnS		McDonald-CE		Sun
Ion	$\log(N/N_{\rm tot})$	n	$\log(N/N_{\rm tot})$	n	$\log(N/N_{\rm tot})$
He I	-0.58 ± 0.16	9	-0.54 ± 0.15	3	-1.11
C I	-2.78 ± 0.17	10			-3.65
C II	-2.69 ± 0.14	15	-2.88 ± 0.16	4	-3.65
N I	-2.60 ± 0.20	3			-4.26
N II	-3.00 ± 0.17	21	-3.01 ± 0.18	9	-4.26
O I	-2.82 ± 0.13	11	-2.74 ± 0.19	2	-3.38
O II	-3.28 ± 0.22	9			-3.38
Ne I	-3.22 ± 0.06	4			-4.20
Na I	-4.22 ± 0.24	2			-5.87
Mg I	-3.62 ± 0.20	1			-4.51
Mg II	-3.73 ± 0.12	4			-4.51
Al II	-5.32 ± 0.11	7			-5.67
Al III	-5.10 ± 0.09	4			-5.67
Si II	-4.28 ± 0.23	9	-4.23 ± 0.11	2	-4.53
Si III	-3.96 ± 0.22	2			-4.53
P II	-5.81 ± 0.12	8	-5.76 ± 0.13	3	-6.68
S II	-4.43 ± 0.18	48	-4.47 ± 0.17	21	-4.90
Cl II	-6.35 ± 0.20	1	-6.47 ± 0.20	1	-6.54
Ar II	-5.03 ± 0.05	4	-4.96 ± 0.19	2	-5.86
Ti II	-6.70 ± 0.04	5			-7.14
Cr II	-6.01 ± 0.07	5	-5.89 ± 0.14	2	-6.40
Fe II	-4.08 ± 0.16	63	-4.16 ± 0.18	31	-4.59
Sr II	-8.50 ± 0.20	1			-9.12

4.1. Light elements: C to Ar

Carbon is enhanced by ~0.9 dex in comparison with the solar abundance and does not show strong evidence of vertical abundance stratification (see Fig. 1a). Nitrogen appears to be strongly enhanced by ~1.7 dex for the neutral species and by ~1.3 dex for the first ion. Unlike C, it shows signatures of vertical abundance stratification (see Fig. 2a). The abundances inferred from singly-ionized oxygen is almost the same as its solar value, while the neutral species is enhanced by ~0.5 dex.

Neon and argon appear to be enhanced respectively by ~1.0 dex and ~0.8 dex in comparison with their solar abundances. The sodium abundance is estimated from the analysis

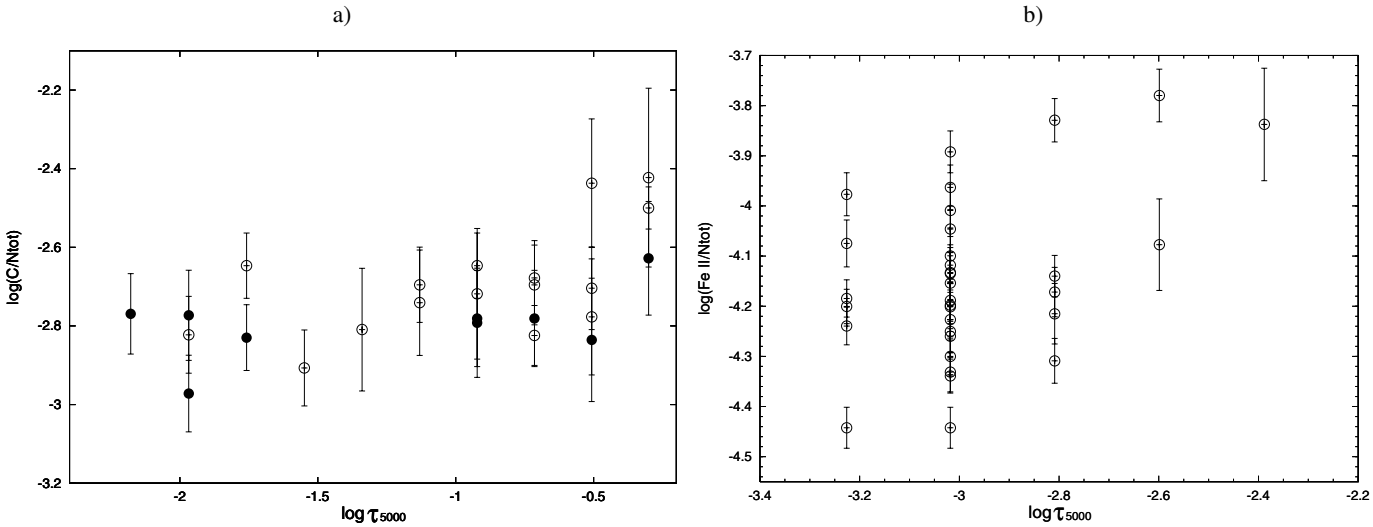

Fig. 1. Abundance estimates from the analysis of a) C I (filled circles) and C II (open circles) and b) Fe II (open circles) line profiles as a function of line (core) formation optical depth. No clear signatures of abundance stratification are visible. The abundances obtained have approximately the same value for all optical depths at which carbon lines are formed.

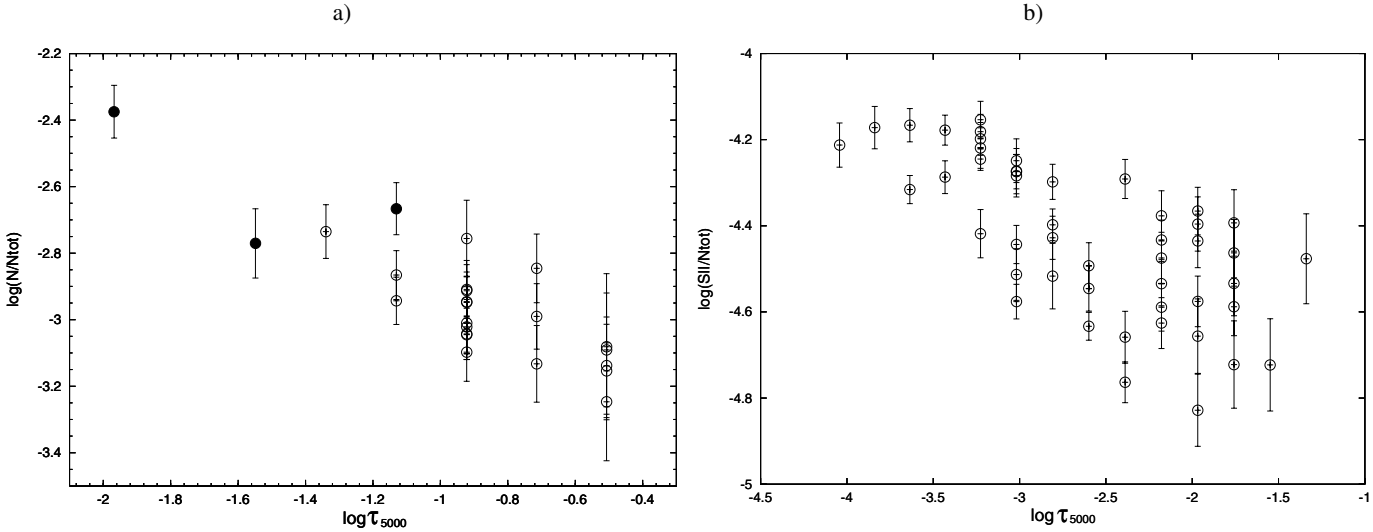

Fig. 2. Same as in Fig. 1 but for a) nitrogen and b) singly ionized sulfur. N I (filled circles) and N II (open circles) lines which are formed in layers with $\log \tau_{5000} < -1.0$ require an enhanced abundance to be fit in comparison with lines of the same ionization stage formed deeper in the atmosphere. A similar situation is found for S II (open circles) lines formed in layers with $\log \tau_{5000} < -1.5$.

of two comparatively weak Na I lines at 5688.205 Å and 8194.824 Å, which results in a ∼1.6 dex enhancement.

Only one unblended Mg I line (5172.684 Å) was found, which results in a magnesium enhancement of ∼0.9 dex. Meanwhile, singly ionized magnesium is enhanced by ∼0.8 dex. Al II and Al III are slightly enhanced by ∼0.3 dex and ∼0.5 dex respectively. Singly ionized silicon has only a ∼0.2 dex enhancement in comparison with its solar abundance, while Si III is enhanced by ∼0.6 dex. Phosphorus shows ∼0.9 dex enhancement. Sulfur appears to be vertically stratified like nitrogen (see Fig. 2b) and its average atmospheric abundance is enhanced by ∼0.4 dex. Chlorine seems to have a solar abundance.

4.2. Iron-group elements: Ti to Fe

The spectrum of HD 135485 is extremely rich in Fe II lines. Many of them originate from high-excitation levels with $E_i \geq 10$ eV. For Fe II lines, we have used mainly Raassen & Uylings (1998) results to specify their oscillator strengths and the VALD-2 database to specify the damping coefficients. The Raassen & Uylings (1998) oscillator strength data usually provides a slightly better agreement between observed and simulated Fe II line profiles than the Kurucz (1993) GFIRON list (Pickering et al. 2001; Ryabchikova et al. 2005). The obtained average atmospheric Fe II abundance is enhanced by ∼0.5 dex and shows some signs of stratification (see Fig. 1b), but in an opposite manner to nitrogen and sulfur (i.e. with the concentration *increasing* toward deeper layers).

Using the ESPaDOnS spectra we find that chromium and titanium are represented by only a few unblended lines and both elements appear to be enhanced by ∼0.4 dex. The oscillator strengths for Cr II lines have been taken from Raassen & Uylings (1998), while for Ti II lines we have used VALD-2 database.

We also checked the Sr II line at 4077.71 Å, which is only marginally visible in these spectra. Its abundance analysis reveals a ∼0.6 dex enhancement – much less than the

value 1.24 dex enhancement obtained by Trundle et al. (2001). Nevertheless, the enhancements of the other chemical species reported in Table 3 are in good agreement with the results of Trundle et al. (2001).

Adoption of different values of microturbulent velocity by Trundle et al. (2001) and by us should lead to systematic differences in our derived abundance. However, these differences may be reduced because we have used different line lists and atomic data for the abundance analysis. Trundle et al. (2001) have used mostly NIST atomic data for all chemical species, while we have tried to use the most precise atomic data currently available for each element (see Table 2).

5. Vertical abundance stratification

Applying the technique described in Sect. 3.2 we have tried to determine if the abundances of some chemical species are vertically stratified. To reach this aim, we need to analyze as many line profiles with different depths of formation (characterised by different excitation potential and line strength) as possible. According to Table 3, a comprehensive analysis can only be performed for carbon, nitrogen, oxygen, sulfur and iron, which are represented in the spectrum of HD 135485 by a sufficient number of lines. In general, we have selected for our analysis lines free of predicted or inferred blends. However, if a blend is from a line of the same chemical element that forms the main line profile, such a line was also included in our simulation.

The very sharp absorption lines of the HD 135485 (8 to 15 bins per line profile), the relatively low signal-to-noise ratio and the uncertainties in the atomic data provide comparatively high errors in abundances inferred from a single line. Taking into account these uncertainties as well as ionization balance errors, we can still see some tendencies of vertical abundance stratification for some of the analyzed chemical elements. Figure 2 shows a systematic trend, wherein N and S lines formed higher in the atmosphere provide abundances which are significantly larger than those formed lower in the atmosphere. To check the influence of differences in $\log gf$ values in different databases we have performed independent simulations of sulfur lines using NIST and VALD2 atomic data and have found similar systematic trends in both cases.

The trend observed in the abundances of N and S was previously reported by Trundle et al. (2001), but they interpreted it in terms of microturbulence. However, such an interpretation would require a similar behaviour of the lines of C, O and Fe, which we do not observe. For example, although the inferred nitrogen and sulfur abundances appear to increase systematically with line strength, carbon and oxygen abundances are approximately constant, whereas the iron abundance shows a weak tendency to decrease with line strength (see Fig. 1). The lack of a coherent trend in the abundances derived from weak versus strong lines in spectra of different elements is not consistent with a microturbulent interpretation, and is fully consistent with chemical stratification. Our simulations of Fe II lines show that adoption of a microturbulent velocity $\xi = 2$ km s^{-1} results in well visible decreasing of iron abundance with line strength. We point out that this conclusion does not necessarily imply that microturbulence is not present, but rather that it cannot explain the observed systematic abundance trends, that its presence is not implied by any of the data discussed in this paper, and that its presence would be surprising given published observational and theoretical results (Landstreet 1998). Our results therefore suggest that the observed systematic trends in the abundances of N and S imply that these elements are vertically stratified in the atmosphere of HD 135485.

To obtain an estimate of the abundance distribution as a function of optical depth for N and S, we have employed a two-zone empirical model with a transition zone (Ryabchikova et al. 2003; Wade et al. 2003) and analyzed simultaneously the same list of lines selected for each element. The final results for nitrogen and sulfur stratification in the atmosphere of HD 135485 are presented in Table 4 and are illustrated in Fig. 3. They are in a good accordance with the abundance stratification data that we have obtained from the first method for N and S (see Fig. 2). For comparison, we have also simulated the same list of lines assuming the same abundance of the element (fitted as a free parameter) at different atmospheric depths. From the last two columns in Table 4 we can see that the model with stratified abundance distribution results in a 30% lower χ^2-function than the model with uniform abundance. This fact shows that application of stratified model significantly improves our fit of analysed line profiles.

The N and S abundance stratifications were also inferred assuming other stellar atmosphere models with the same gravity $\log g = 4.0$, but with the different effective temperatures $T_{\rm eff} = 14\,500$ K and $T_{\rm eff} = 16\,500$ K, to estimate the influence of effective temperature errors on the vertical abundance stratification profiles. Our simulations show that an effective temperature increase does not effect the final results, while its decrease leads to significant changes of the vertical abundance stratification profile. The stellar atmosphere model with lower temperature results in a steeper stratification profile for S and an increase in the average S abundance by 0.4 dex, while for nitrogen it provides approximately a 0.8 dex increase in abundances derived from lines formed deeper in the atmosphere where $\log \tau_{5000} > -1.0$. This leads to a reversed stratification profile for N. Therefore the results obtained (see Table 4) for sulfur can be considered to be a lower limit for its abundance stratification profile, whereas a uniform vertical distribution of N cannot be ruled out.

In conclusion, the analysis of our spectra shows vertical stratification of of S and possibly N, while the elements C, O, Ne, Ar, Cr and Ti seem to have an homogeneous abundance throughout the parts of the atmosphere that we can sample. Meanwhile, we cannot draw firm conclusions concerning the stratification of Fe, Mg, Si, P and Al. Some of these elements are represented by a small number (see Table 3) of unblended line profiles and it is hard to obtain clear results.

6. Discussion

According to Trundle et al. (2001), HD 135485 is an evolved star that probably belongs to the BHB group. Its slow rotation, high effective temperature ($T_{\rm eff} = 15\,500$ K) and observed abundance anomalies (see Table 3) support the idea that microscopic atomic diffusion is effective in its atmosphere.

Our analysis suggests that sulfur is moderately overabundant and increases in concentration in the upper atmospheric layers. Nitrogen is strongly overabundant and shows a similar signature of vertical stratification, although the derived stratification of this element depends sensitively on the adopted effective temperature (which is uncertain by about ±1000 K). Similar results for these two species were obtained earlier by Trundle et al. (2001), but explained in terms of a microturbulent velocity field. Absence of any abundance stratification for several other elements as well as some hints that the iron abundance might be enhanced in deeper atmospheric layers (i.e. opposite to the tendency shown by N and S) shows that this interpretation is not able to correctly explain the spectroscopic properties of this star. A more plausible

Table 4. Parameters of the vertical abundance distribution. Here the columns specify respectively the element, its abundance in deeper layers, the abundance difference between the two boundaries, the optical depth τ_1 of the transition zone's lower (deeper) boundary, where the element's abundance increases (or decreases) linearly, the optical depth τ_2 of the transition zone's upper boundary, the radial velocity and $v \sin i$ with the respective error estimates and the fit quality for the model with abundance stratification χ^2_s and without it χ^2_n.

El.	Abundance in $\log(N/N_{tot})$		Atmospheric depths in $\log \tau_{5000}$		V_r	$V \sin i$		
	Low atmosphere	Abundance difference	$\log \tau_1$	$\log \tau_2$	km s^{-1}	km s^{-1}	χ^2_s	χ^2_n
N	-3.15 ± 0.03	0.68 ± 0.25	-0.67 ± 0.27	-2.75 ± 0.45	-4.20 ± 0.13	1.3 ± 0.7	2.61	3.83
S	-4.63 ± 0.02	0.94 ± 0.28	-1.31 ± 0.16	-3.00 ± 0.40	-4.24 ± 0.08	3.0 ± 1.2	6.87	10.06

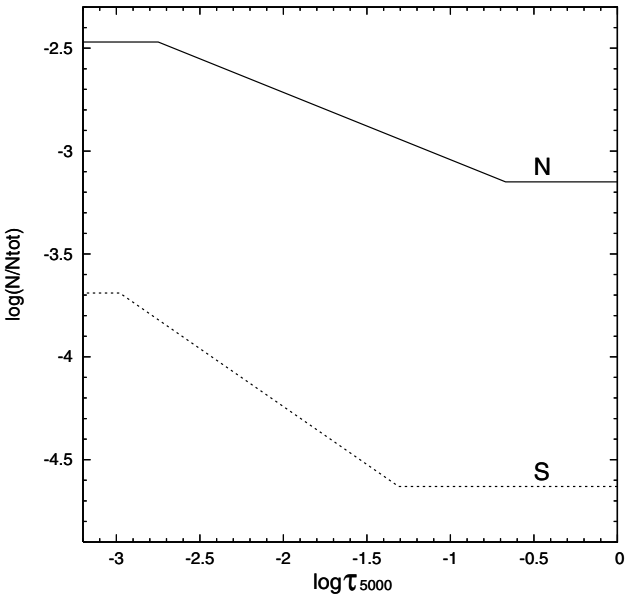

Fig. 3. Abundance stratification in the atmosphere of HD 135485 for nitrogen and sulfur.

explanation is that the abundances of N and S vary as a function of depth within the atmosphere. The detection of a similar trend of Fe abundance versus depth in the BHB star WF4-3085 in the globular cluster M 13 (Khalack et al. in preparation) suggests that the trends observed in HD 135485 for N and S, and possibly Fe, are real. These facts can be considered as further arguments in support of the efficiency of atomic diffusion in the atmosphere of HD 135485, and possibly in the atmospheres of BHB stars generally.

The study of chemical stratification in the atmospheres of BHB stars is a recent field of research. Previously Bonifacio et al. (1995) reported the possibility of helium stratification in the atmosphere of Feige 86. The results obtained here for nitrogen and sulfur stratification in HD 135485 are the first report of stratification of metal species in a BHB star. An extensive search for vertical stratification for a large number of chemical species in the atmospheres of BHB stars with a range of $T_{\rm eff}$ would be very useful to place constraints on model atmospheres in which the atmospheric structure is calculated self-consistently with the stratification predicted by the diffusion phenomenon, such as those of Hui-Bon-Hoa, LeBlanc & Hauschildt (2000). To obtain more precise results from observations pertaining to stratification of the elements, such models should be used since stratification can modify the atmospheric structure and thus the inferred stratification obtained by spectral analysis. For example, we found that the nitrogen stratification for HD 135485 is quite sensitive to the $T_{\rm eff}$ used for the underlying model atmosphere.

Acknowledgements. This research was partially funded by the Natural Sciences and Engineering Research Council of Canada (NSERC). We thank the Réseau québécois de calcul de haute performance (RQCHP) for computing resources. GAW acknowledges support from the Academic Research Programme (ARP) of the Department of National Defence (Canada). BBB thanks the staff of McDonald Observatory for their assistance in collecting the CE data, and the National Research Council and Naval Research Laboratory for recent salary support. We are grateful to Dr. T.Ryabchikova for helpful discussions and suggestions.

References

Asplund, M., Grevesse, N., & Sauval, A. J. 2005 in Cosmic Abundances as Records of Stellar Evolution and Nucleosynthesis, ed. T. G. Barnes, & F. N. Bash, ASP Conf. Ser., 336, 25
Behr, B. B. 2003, ApJS, 149, 101
Behr, B. B., Djorgovski, S. G., & Cohen, J. G., et al. 2000, ApJ, 528, 849
Bonifacio, P., Castelli, F., & Hack, M. 1995, A&AS, 110, 441
Donati, J.-F., Semel, M., Carter, B., et al. 1997, MNRAS, 291, 658
Donati, J.-F., Catala, C., Wade, G. A., et al. 1999, A&AS, 134, 149
Dufton, P. L. 1973, A&A, 28, 267
Deupree, R. G., & Wallace, R. K. 1987, ApJ, 317, 724
Ferraro, F. R., Paltrinieri, B., Fusi Pecci, F., et al. 1998, ApJ, 500, 311
Fuhr, J. R., & Wiese, W. L. 2006, J. Phys. Chem. Ref. Data, in press
Gies, D. R., & Lambert, D. L. 1992, ApJ, 387, 673
Glaspey, J. W., Michaud, G., Moffat, A. F. J., & Demers, S. 1989, ApJ, 339, 926
Grundhal, F., Catelan, M., Landsman, W. B., et al. 1999, ApJ, 524, 242
Hauschildt, P. H., Baron, E., & Allard, F. 1997, ApJ, 483, 390
Hui-Bon-Hoa, A., LeBlanc, F., & Hauschildt, P. H. 2000, ApJ, 535, L43
Khalack, V., Wade, G. 2006, A&A, 450, 1157
Khalack, V., LeBlanc, F., et al., in preparation
Kupka, F., Piskunov, N. E., Ryabchikova, T. A., et al. 1999, A&AS, 138, 119
Kurucz, R. L. 1993, CDROMs 13, 22, 23, SAO, Cambridge
Landstreet, J. D. 1988, ApJ, 326, 967
Landstreet, J. D. 1998, Contrib. Astron. Obs. Scalnaté Pleso, 27, 350
Lehner, N., Dufton, P. L., Lambert, D. L., et al. 2000, MNRAS 314, 199
McCarthy, J. K. 1990, in Proc. 2nd ESO/ST-ECF Data Analysis Workshop, (Garching: ESO), 119
McCarthy, J. K., Sandiford, B. A., Boyd, D., & Booth, J. 1993, PASP, 105, 881
Peterson, R. C., Rood, R. T., & Crocker, D. A. 1995, ApJ, 453, 214
Pickering, J. C., Johansson, S., & Smith, P. L. 2001, A&A, 377, 361
Press, W. H., Teukolsky, S. A., Vetterling, W. T., & Flannery, B. P. 1992, Numerical recipes in C: the art of scientific computing, 2nd ed. (Cambridge University Press), 995
Raassen, A. J. J., & Uylings, P. H. M. 1998, A&A, 340, 300
Reader, J., Wiese, W. L., Martin, W. C., et al. 2002, NASA Laboratory Astrophysics Workshop, ed. F. Salama, Ref. Conf. Proc.: NASA/CP-2002-21186, 80
Recio-Blanco, A., Piotto, G., Aparicio, A., & Renzini, A. 2004, A&A, 417, 597
Ryabchikova, T. A., Piskunov, N. E., Stempels, H. C., Kupka, F., & Weiss, W. W. 1999, in Proc. of the 6th International Colloquium om Atomic Spectra and Oscillator Strengths, Victoria BC, Physica Scripta T83, 162
Ryabchikova, T. A., Wade, G. A., & LeBlanc, F. 2003, in Proc. of the Conference at University of North-West, Mmabatho, South Africa, ed. L. A. Balona, H. F. Henrichs, & R. Medupe, ASP Conf. Proc., 305, 181
Ryabchikova, T., Leone, F., & Kochukhov, O. 2005, A&A, 438, 973
Schönberner, D. 1973, A&A, 28, 443
Shortridge, K. 1993, The Figaro 2.4 Manual
Trundle, C., Dufton, P. L., Rolleston, W. R. J., et al. 2001, MNRAS, 328, 291
Wade, G. A., LeBlanc, F., Ryabchikova, T. A., & Kudryavtsev, D. 2003, in Proc. of 210th IAU Symp on Modelling of Stellar Atmospheres, ed. N. Piskunov, W. W. Weiss, & D. F. Gray, Published on behalf of the IAU by the Astronomical Society of the Pacific, D7
Wade, G. A., Bagnulo, S., Kochukhov, O., et al. 2001, A&A, 374, 265

Online Material

Table 2. List of spectral lines used for the abundance analysis.

λ, Å	$\log gf$	E_i, cm^{-1}	$\log \gamma_{\rm rad}$	Ref.
		H I		
4026.186	−0.701	169086.76	appx	NIST
4026.198	−0.972	169086.84	appx	NIST
4120.811	−1.738	169086.76	appx	NIST
4387.929	−0.883	171134.89	appx	NIST
4437.553	−2.034	171134.89	appx	NIST
4471.474	−0.278	169086.76	appx	NIST
4471.489	−0.550	169086.84	appx	NIST
4713.139	−1.230	169086.76	appx	NIST
4921.931	−0.435	171134.89	appx	NIST
5015.678	−0.820	166277.44	appx	NIST
5047.739	−1.601	171134.89	appx	NIST
		C I		
4371.367	−1.962	61981.82	appx	NIST
4771.742	−1.866	60393.14	appx	NIST
4932.039	−1.658	61981.82	appx	NIST
5380.337	−1.616	61981.82	appx	NIST
7113.179	−0.773	69744.03	appx	NIST
7115.168	−0.934	69710.66	appx	VALD
7116.988	−0.907	69744.03	appx	VALD
9061.433	−0.346	60352.63	appx	VALD
9078.288	−0.581	60352.63	appx	VALD
9088.515	−0.429	60352.63	appx	VALD
9111.809	−0.298	60393.14	appx	VALD
9658.431	−0.280	60393.14	appx	VALD
		C II		
3918.968	−0.533	131724.37	8.98	NIST
4267.261	−0.584	145550.70	9.39	NIST
4267.261	0.716	145550.70	9.39	NIST
4313.106	−0.373	186443.69	appx	NIST
5132.947	−0.211	166967.13	8.95	NIST
5137.257	−0.911	166967.13	8.95	NIST
5139.174	−0.707	166990.73	8.95	NIST
5535.353	−1.493	157234.07	8.94	NIST
5648.072	−0.424	166990.73	8.94	VALD
5662.459	−0.249	167035.71	8.94	VALD
5891.597	−0.440	145549.27	appx	VALD
6098.512	0.226	182043.41	appx	VALD
6779.940	0.025	166990.73	8.93	NIST
6783.908	0.304	167035.71	8.93	VALD
7231.337	0.043	131724.37	appx	VALD
7237.166	−0.656	131735.52	appx	VALD
		N I		
6482.699	−0.510	94881.82	appx	VALD
7442.298	−0.385	83317.83	8.64	VALD
7898.982	0.024	99663.43	appx	VALD
7899.284	−0.911	99663.91	appx	VALD
		N II		
4447.030	0.228	164610.76	9.16	NIST
4507.556	−0.817	166678.64	9.33	VALD
4601.478	−0.428	148940.17	9.23	VALD
4613.868	−0.665	148940.17	9.23	VALD
4621.396	−0.514	148940.17	9.23	VALD
4630.539	0.094	149076.52	9.15	VALD
4779.722	−0.587	166521.69	9.58	VALD
4803.287	−0.113	166678.64	9.58	VALD
4987.376	−0.555	168892.21	9.34	VALD
4994.367	−0.069	168892.21	9.34	VALD
5001.135	0.263	166521.69	8.45	VALD
5001.475	0.439	166582.45	8.45	VALD
5005.150	0.592	166678.64	8.25	VALD
5007.333	0.171	168892.21	9.33	VALD
5010.621	−0.606	148940.17	9.22	VALD
5025.659	−0.546	166678.64	8.43	VALD
5480.050	−0.756	170666.23	9.34	VALD
5676.020	−0.368	148908.59	9.14	VALD

Table 2. continued.

λ, Å	$\log gf$	E_i, cm^{-1}	$\log \gamma_{\rm rad}$	Ref.
5679.554	0.250	149076.52	9.13	VALD
5686.212	−0.549	148940.17	9.22	VALD
5941.650	0.313	170666.23	9.59	VALD
		O I		
4368.242	−1.964	76794.98	8.76	NIST
5329.681	−1.473	86627.78	7.54	NIST
5329.690	−1.268	86627.78	7.54	NIST
5330.735	−1.570	86631.45	7.55	VALD
5330.741	−0.983	86631.45	7.55	VALD
6155.961	−1.363	86625.76	7.60	NIST
6155.971	−1.011	86625.76	7.61	NIST
6155.989	−1.120	86625.76	7.61	NIST
6158.172	−0.995	86631.45	7.62	NIST
6158.177	−0.409	86631.45	7.61	NIST
6454.444	−1.066	86627.78	7.66	NIST
7001.922	−1.011	86630.59	7.93	NIST
7002.230	−0.741	86631.15	7.93	NIST
7156.701	0.288	102662.03	8.76	NIST
7254.448	−1.054	88631.15	7.59	NIST
7254.531	−1.753	88631.30	7.59	NIST
8446.758	0.014	76794.98	8.77	NIST
8820.423	0.379	102662.03	8.74	NIST
		O II		
4069.882	0.344	206786.297 8.48		NIST
4072.157	0.552	206877.86	8.50	NIST
4119.216	0.452	208484.20	9.09	NIST
4414.899	0.172	189068.51	9.46	NIST
4641.810	0.055	185340.58	8.96	NIST
4649.135	0.308	185499.12	8.96	NIST
4650.838	−0.362	185235.28	8.96	NIST
4661.632	−0.278	185340.58	8.96	NIST
4676.235	−0.394	185499.12	8.96	NIST
		Ne I		
7488.871	0.167	148257.79	7.95	NIST
7535.774	0.040	148257.79	8.12	NIST
8377.608	0.680	149657.04	8.01	NIST
8654.383	0.544	150858.51	8.03	NIST
		Na I		
5688.205	−0.452	16973.37	appx	NIST
8183.255	0.237	16956.17	appx	NIST
		Mg I		
5172.684	−0.393	21870.46	7.99	NIST
		Mg II		
4390.572	−0.523	80650.02	appx	NIST
4433.988	−0.907	80650.02	appx	NIST
7877.054	0.391	80619.50	appx	NIST
7896.366	0.643	80650.02	appx	NIST
		Al II		
4663.046	−0.284	85481.35	7.99	VALD
5593.300	0.410	106920.56	appx	VALD
6243.203	−0.080	105470.93	appx	VALD
6243.367	0.670	105470.93	appx	VALD
6823.390	−0.140	105441.50	appx	VALD
6837.130	0.080	105470.93	appx	VALD
6920.343	−0.160	105470.93	appx	VALD
7471.410	0.780	110089.83	appx	VALD
		Al III		
4512.565	0.410	143633.38	appx	VALD
4529.189	0.660	143713.50	appx	VALD
5696.604	0.230	126164.05	appx	VALD
5722.730	−0.070	126164.05	appx	VALD
		Si II		
4128.054	0.306	79338.50	9.44	NIST
4130.872	−0.840	79355.02	9.44	NIST
4130.894	0.464	79355.02	9.44	NIST
4621.722	−0.390	101024.35	9.01	NIST
5055.984	0.440	81251.32	9.04	NIST

Table 2. continued.

λ, Å	$\log gf$	E_i, cm^{-1}	$\log \gamma_{\rm rad}$	Ref.
5466.849	−1.340	101024.35	9.02	NIST
5466.894	−0.030	101024.35	9.02	NIST
5669.563	0.690	114530.87	8.07	VALD
5868.444	0.400	117176.37	8.04	VALD
5957.560	−0.350	81191.34	8.82	NIST
7849.618	−0.810	101024.35	9.04	NIST
7849.722	0.490	101024.35	9.04	NIST
		Si III		
4552.622	0.292	153377.05	9.08	NIST
4574.757	−0.406	153377.05	9.08	NIST
		P II		
4420.712	−0.478	88893.22	8.29	NIST
4499.230	0.377	107922.93	8.27	NIST
4602.069	0.799	103667.86	8.25	NIST
5296.077	−0.134	87124.60	8.13	NIST
5344.729	−0.390	86597.55	8.12	NIST
5425.880	0.241	87124.60	8.11	NIST
6043.080	0.384	87124.60	8.01	NIST
6459.945	0.101	88192.13	7.96	NIST
		S II		
4028.750	0.000	128599.16	8.60	NIST
4032.768	0.240	131028.85	9.38	NIST
4142.259	0.240	127825.08	8.62	NIST
4153.068	0.620	128233.20	8.52	NIST
4162.665	0.780	128599.16	8.62	NIST
4165.100	0.060	140230.10	9.21	NIST
4168.384	−0.160	127976.34	8.63	NIST
4217.182	−0.150	128599.16	8.49	NIST
4257.379	0.360	140750.34	9.24	NIST
4267.762	0.290	129858.18	8.71	NIST
4269.725	0.080	129787.83	8.66	VALD
4278.506	−0.114	129787.83	8.66	NIST
4282.593	−0.010	129858.18	8.64	NIST
4294.402	0.549	130134.16	8.62	VALD
4432.368	−0.470	127976.34	8.68	NIST
4456.382	−0.560	127825.08	8.74	VALD
4463.581	0.134	128599.16	8.73	VALD
4486.634	−0.400	127976.34	8.76	NIST
4716.271	0.410	109831.59	8.88	NIST
4792.007	0.306	130134.16	8.74	VALD
4815.552	0.090	110268.60	8.87	NIST
4819.445	−0.490	129787.83	8.66	NIST
4819.626	−0.220	130641.11	8.93	NIST
4835.846	−0.990	129858.18	8.64	VALD
4885.648	−0.610	112937.57	8.75	NIST
4900.513	−0.490	129858.18	8.72	VALD
4901.277	−0.460	130134.16	8.66	VALD
4917.198	−0.320	112937.57	8.76	NIST
4925.343	−0.235	109560.69	8.86	VALD
4942.473	−0.960	109560.69	8.87	NIST
4991.969	−0.246	109831.59	8.85	VALD
5009.567	−0.280	109831.59	8.86	NIST
5014.042	0.030	113461.54	8.75	VALD
5027.203	−0.710	105599.06	8.75	NIST
5032.434	0.270	110268.60	8.85	NIST
5103.332	−0.275	110268.60	8.84	VALD
5142.322	−0.820	106044.24	8.70	NIST
5201.027	0.090	121528.72	9.16	NIST
5320.723	0.490	121530.02	9.09	NIST
5428.655	−0.120	109560.69	8.88	VALD
5453.855	0.557	110268.60	8.85	VALD
5509.705	−0.117	109831.59	8.88	VALD
5564.958	−0.320	110268.60	8.86	NIST
5616.633	−0.640	110177.02	8.60	NIST
5639.977	0.330	113461.54	8.75	VALD
5647.020	0.110	112937.57	8.75	VALD
5819.254	−0.760	113461.54	8.76	NIST

Table 2. continued.

λ, Å	$\log gf$	E_i, cm^{-1}	$\log \gamma_{\rm rad}$	Ref.
6305.482	−0.190	114279.33	8.28	NIST
		Cl II		
4794.556	0.455	107879.66	appx	VALD
		Ar II		
4426.001	0.158	135086.00	appx	NIST
4609.567	0.304	148842.47	appx	NIST
4806.020	0.210	134241.74	appx	NIST
4879.863	0.296	138243.64	appx	NIST
		Ti II		
4300.049	−0.490	9518.06	8.47	VALD
4443.794	−0.700	8710.44	8.20	VALD
4501.273	−0.760	8997.71	8.20	VALD
4563.761	−0.790	9850.90	8.22	VALD
4571.985	−0.230	12676.97	8.37	VALD
		Cr II		
4558.650	−0.449	32854.31	8.41	VALD, R&U
4558.783	−2.530	32859.07	8.41	VALD, R&U
4588.199	−0.627	32836.68	8.41	VALD, R&U
4616.539	−2.020	91576.30	8.92	VALD, R&U
4616.629	−1.361	32844.76	8.41	VALD, R&U
4634.070	−0.990	32844.76	8.41	VALD, R&U
5237.329	−1.350	32854.31	8.40	VALD, R&U
5237.329	−0.740	86785.36	8.85	VALD, R&U
		Fe II		
4044.012	−2.671	44929.55	8.70	R&U
4048.832	−2.381	44917.07	8.73	R&U
4048.931	−2.779	73603.50	8.99	R&U
4173.461	−2.617	20830.58	8.61	VALD
4173.473*	−2.185	24333.78	8.51	VALD, F&W
4178.862	−2.535	20830.58	8.49	R&U
4233.172	−1.947	20830.58	8.61	R&U
4258.154	−3.478	21812.06	8.48	R&U
4273.326	−3.303	21812.06	8.62	R&U
4296.572	−2.933	21812.06	8.49	R&U
4303.176	−2.511	21812.06	8.61	R&U
4351.769	−2.216	21812.06	8.61	R&U
4385.381	−2.581	22409.85	8.62	R&U
4416.830	−2.602	22409.85	8.61	R&U
4461.706	−2.065	50212.83	8.62	R&U
4489.183	−2.971	22810.36	8.49	R&U
4491.405	−2.755	23031.30	8.48	R&U
4508.214	−2.589	63948.79	9.01	R&U
4508.288	−2.349	23031.30	8.62	R&U
4515.339	−2.540	22939.36	8.49	R&U
4522.634	−2.169	22939.36	8.61	R&U
4541.524	−2.973	23031.30	8.61	R&U
4555.893	−2.421	22810.36	0.85	R&U
4576.340	−2.976	22939.36	8.61	R&U
4582.835	−3.224	22939.36	8.49	R&U
4583.837	−1.867	22637.21	8.61	R&U
4596.015	−1.956	50212.83	8.74	R&U
4629.339	−2.478	22637.21	8.48	R&U
4635.316	−1.578	48039.09	8.73	R&U
4731.453	−3.127	23317.63	8.61	R&U
4951.584	0.198	83136.49	8.96	R&U
5001.864*	0.010	31302.42	7.97	VALD, F&W
5001.959	0.916	82978.68	8.93	R&U
5004.195	0.504	82853.66	8.93	R&U
5018.440	−1.345	23317.63	8.49	R&U
5030.630	0.433	82978.68	9.02	R&U
5032.712	0.107	83812.32	8.99	R&U
5035.708	0.639	82978.68	8.94	R&U
5061.718	0.290	83136.49	9.05	R&U
5070.899	0.275	83136.49	9.02	R&U
5075.764	0.168	84326.91	8.94	R&U
5097.271	0.315	83713.54	8.94	R&U
5144.355	0.295	84424.37	8.99	R&U

Table 2. continued.

λ, Å	$\log gf$	E_i, cm^{-1}	$\log \gamma_{\rm rad}$	Ref.
5149.465	0.544	84266.56	8.92	R&U
5169.033	−1.250	23317.63	8.49	R&U
5197.568	−2.105	83865.63	9.05	VALD
5197.577	−2.348	26055.42	8.48	R&U
5199.122	0.107	83713.54	9.02	R&U
5216.854	0.480	84710.68	8.96	R&U
5216.863	0.659	84527.78	8.93	R&U
5227.323	0.191	84844.83	8.93	R&U
5227.481	0.834	84296.83	8.91	R&U
5234.615	−2.385	84266.56	8.98	R&U
5234.625	−2.279	25981.63	8.49	R&U
5247.952	0.550	84938.18	8.95	R&U
5260.259	1.069	84035.01	8.91	VALD
5272.397	−2.009	48039.09	8.69	R&U
5276.002	−2.213	25805.33	8.49	R&U
5284.109	−3.195	23317.63	8.53	R&U
5291.666	0.556	84527.78	9.00	R&U
5316.225	0.340	84035.14	8.92	R&U
5316.615	−2.014	25428.78	8.48	R&U
5316.784	−2.783	25981.63	8.61	R&U
5339.585	0.540	84296.83	8.91	R&U
5387.063	0.522	84863.35	8.89	R&U
5429.988	0.438	85462.86	8.93	R&U
5482.308	0.405	85184.73	8.98	R&U
5506.195	0.849	84863.35	8.89	R&U
5780.128	0.413	86124.30	8.96	R&U
5783.630	0.362	86416.33	8.97	R&U
5902.825	0.420	86416.33	9.09	R&U
5961.705	0.678	86124.30	9.20	R&U
		Sr II		
4077.709	0.167	0.00	appx	VALD